



**HAL**  
open science

## An out of the box vision over oxidative chemical vapor deposition of PEDOT involving sublimed iron trichloride

Milad Mirabedin, Hugues Vergnes, Nicolas Caussé, Constantin Vahlas,  
Brigitte Caussat

### ► To cite this version:

Milad Mirabedin, Hugues Vergnes, Nicolas Caussé, Constantin Vahlas, Brigitte Caussat. An out of the box vision over oxidative chemical vapor deposition of PEDOT involving sublimed iron trichloride. *Synthetic Metals*, 2020, 10.1016/j.synthmet.2020.116419 . hal-02733187

**HAL Id: hal-02733187**

**<https://hal.science/hal-02733187>**

Submitted on 8 Jun 2020

**HAL** is a multi-disciplinary open access archive for the deposit and dissemination of scientific research documents, whether they are published or not. The documents may come from teaching and research institutions in France or abroad, or from public or private research centers.

L'archive ouverte pluridisciplinaire **HAL**, est destinée au dépôt et à la diffusion de documents scientifiques de niveau recherche, publiés ou non, émanant des établissements d'enseignement et de recherche français ou étrangers, des laboratoires publics ou privés.

**An out of the box vision over oxidative chemical vapor deposition of  
PEDOT involving sublimed iron trichloride**

Milad Mirabedin<sup>a, b</sup>, Hugues Vergnes<sup>a</sup>, Nicolas Causse<sup>b</sup>,

Constantin Vahlas<sup>b</sup>, Brigitte Caussat<sup>a\*1</sup>

<sup>a</sup> Laboratoire de Génie Chimique, Université de Toulouse, 4 allée Emile Monso, 31030

Toulouse cedex 4, France.

<sup>b</sup> CIRIMAT, Université de Toulouse, 4 allée Emile Monso, 31030 Toulouse cedex 4, France.

**Abstract**

Oxidative chemical vapor deposition (oCVD) is an efficient technique to produce highly conductive films of Poly (3,4-ethylenedioxythiophene) (PEDOT). Despite numerous studies on the oCVD of PEDOT films, there is limited information on the stability of the sublimation of solid oxidants and on their impact on the polymerization reactions. In this work, we use an *in situ* Quartz Crystal Microbalance to monitor film formation over time. Through a series of deposition experiments between 20 °C and 100 °C and for FeCl<sub>3</sub>/EDOT **molar** gas ratios between 17.3 and 75.3, we analyze in detail the correlations between process parameters and film morphology, composition, surface topography and electrical conductivity on 10 cm silicon wafers. By using multiple substrates at different positions into the reactor, we demonstrate that the formation of PEDOT occurs uniformly through purely surface reactions, following step growth polymerization principles. These results pave the way towards highly conductive oCVD PEDOT films processed from convenient solid oxidants.

**Keywords:** oxidative chemical vapor deposition, PEDOT, thin films, FeCl<sub>3</sub>, conductive polymers.

---

<sup>1</sup> Corresponding author: [brigitte.caussat@ensiacet.fr](mailto:brigitte.caussat@ensiacet.fr) – Phone: +33 534323632 – Fax: +33 534323700

## 1. Introduction

Poly (3,4-ethylenedioxythiophene) (PEDOT) is one of the most significant conductive polymers used in the growing field of organic devices. It is widely used in organic solar cells [1], organic light-emitting diodes (OLEDs) [2], and supercapacitors [3], thanks to its mechanical stability, optical transparency and high electrical conductivity in comparison to other conductive polymers [4]. Its high electrical conductivity (up to 8797 S/cm for single-crystal nanowires [5]) comes from a conjugated bond structure that permits  $\pi$ -orbital overlap along with the alternating double- and single-bonds in the polymer backbone [6].

Since 1990, the main route of PEDOT production has been synthesizing in liquid solution through a series of oxidation and deprotonation steps [7-9]. Vapor phase processes, mainly vapor phase polymerization (VPP) [10] and oxidative chemical vapor deposition (oCVD) [9] have been developed more recently to provide conformal coatings on complex porous substrates and to avoid the substrate-solvent incompatibility in liquid deposition processes. While the VPP process still involves a liquid step, the oCVD is a one-step purely gas phase process where the oxidant serves both to promote monomer polymerization and to subsequently oxidize the neutral polymer to form the conductive, doped polymer. Another advantage of the oCVD is better control over film thickness by varying the deposition time. In the VPP, the polymerization stops when there is no oxidant even if EDOT is still present [11]. By sending oxidant in a controlled manner, oCVD can control the film properties with more precision. Since the introduction of oCVD PEDOT by Gleason and coworkers [9], several solid oxidants have been used to produce films of PEDOT from EDOT monomer. Among them, iron trichloride ( $\text{FeCl}_3$ ) is the most studied one [9,12-14], because of its availability and relatively low toxicity [15,16]. Solid oxidants are commonly placed on a crucible in the reactor and are sublimated at a temperature between 170° C and 350 °C. Despite the wealth of the literature on oCVD PEDOT via  $\text{FeCl}_3$ , the sublimation rate and stability over time have never been reported [9,12-14,17-

24]. These two parameters are important since the sublimation rate of the oxidant allows controlling the gas phase composition and, subsequently, the film's characteristics. The unreacted excess oxidant is often found in as processed PEDOT films, requiring an additional step of post deposition rinsing to improve the electrical conductivity [25]. On the other hand, the control of the stability of the sublimation rate over time is a prerequisite for process implementation. In order to circumvent such sublimation drawbacks [26], solid oxidants have been replaced by more conveniently volatilized liquid ones, such as bromine ( $\text{Br}_2$ ) [19] and later on sulfuric acid ( $\text{H}_2\text{SO}_4$ ) [27], molybdenum(V) chloride ( $\text{MoCl}_5$ ) [28], antimony pentachloride ( $\text{SbCl}_5$ ) [29] and vanadium oxytrichloride ( $\text{VOCl}_3$ ) [29-31].

Despite the advantages of liquid oxidants, there are other issues related to their use, such as **safety**, availability, oxidation efficiency, and subsequent **equipment** corrosion [32]. Consequently, the oCVD of PEDOT from EDOT and solid oxidants, especially  $\text{FeCl}_3$ , remains a promising process, provided sublimation issues are settled [15,16]. This condition comes together with the need to get a better insight into the gas-phase or surface reactions involved between the oxidant and the monomer. Indeed, deposition parameters such as the  $\text{FeCl}_3$ /EDOT ratio in the gas phase are not always detailed in the literature, and except for the **substrate temperature** ( $T_{\text{sub}}$ ), the correlations between the deposition conditions and the film characteristics and properties are not clearly established [9,16,22,23,29,32,33]. As a result, the potential of scaling up the oCVD of PEDOT remains to be more deeply analyzed in terms of film uniformity over large areas. The first effort toward large-scale PEDOT film synthesis has been made by Kovacic et al. who developed a roll-to-roll process [23]. They obtained deposition of PEDOT on  $21 \times 33$  cm pre-cleaned glass slides with a thickness deviation of 5.5% and a conductivity variation of 10% after a post deposition rinsing in methanol. However, they did not correlate process parameters and film uniformity. Except for one study about PEDOT synthesis by oxidative Molecular Layer Deposition [28], no *in situ* measurements of the

deposited mass were published, although they could bring new insights about stability and the gas phase and surface mechanisms involved.

The objective of the present work is to extend the knowledge on the oCVD process yielding PEDOT films from EDOT and FeCl<sub>3</sub> by getting insight into the involved mechanisms. We *in-situ* monitor the deposition of PEDOT using a Quartz Crystal Microbalance (QCM). We analyze in detail the film uniformity over a large scale and establish correlations between key process parameters like precursors ratio and **substrate temperature** and film characteristics, namely thickness, roughness, morphology, chemical composition, and electrical conductivity, both in as-processed and after standard rinsing with methanol.

## 2. Experimental

### 2.1. Materials and methods

oCVD experiments were performed in a custom-built stainless steel reactor (Neyco) schematically represented in Fig. 1a. The optimal reactor geometry is reported to be a substrate-holder placed above the oxidant crucible [34]. Our reactor design is close to those reported in the literature for the oCVD of PEDOT [35], allowing qualitative comparison with reported results [36]. Over and above the conventional design, a Quartz Crystal Microbalance (QCM) with an oscillator (INFICON STM-2) was used for the real-time monitoring of the film deposition to evaluate the mass gain on the substrate per unit time. **The measurement time interval of the QCM was 0.1 s.** The quartz probe was installed inside the vacuum chamber, adjacently to the substrate where the deposition is performed. AT-cut crystals with a nominal frequency of 6 MHz are used with gold electrodes as probes. The decrease in frequency is linearly correlated with the mass gain on the surface of the crystal, **if the deposited layer is not viscoelastic [37]. As PEDOT is a polymeric material, this correlation may not be accurate**

for the present study. For this reason, we only consider QCM frequency changes for observing process stability without converting to the mass. Before each deposition experiment, it was verified that the QCM frequency remains constant under EDOT and N<sub>2</sub> flow. Then, the frequency change due to PEDOT deposition was monitored in real-time.

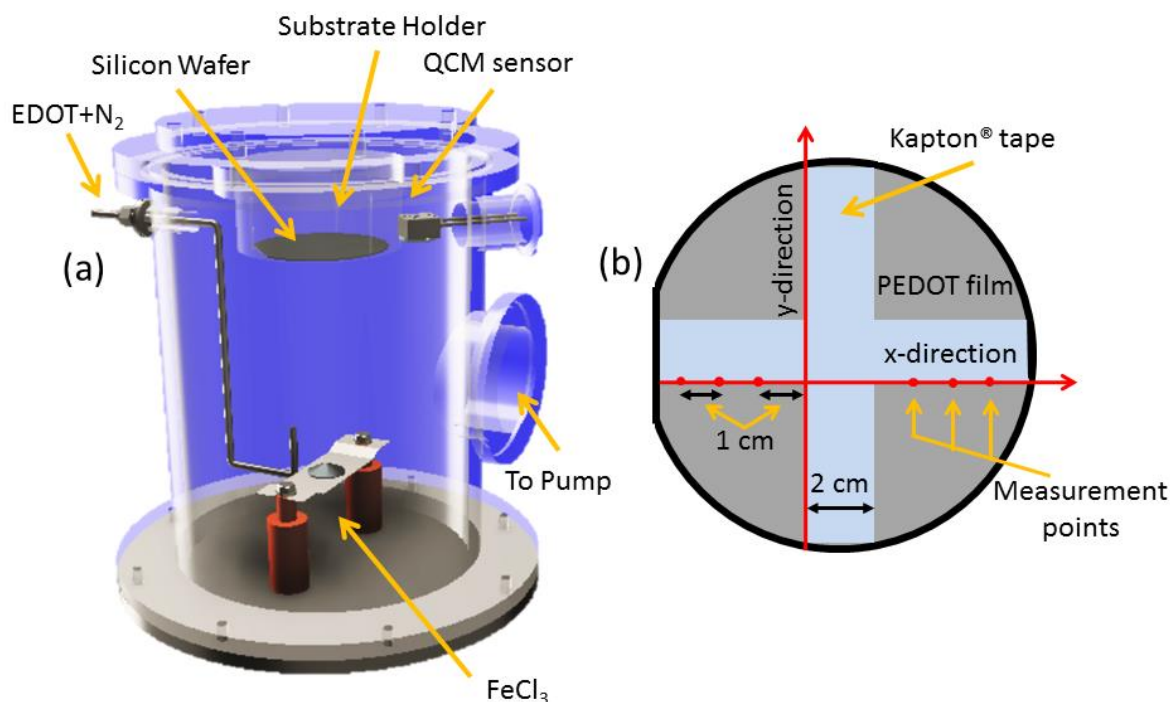


**Fig. 1** Schematic illustration of (a) the oCVD reactor, (b) the substrate, depicting the areas covered by the Kapton® tape, and the thickness measurement points.

## 2.2. Synthesis of poly 3,4-ethylenedioxythiophene (PEDOT via oCVD

3,4-ethylenedioxythiophene (EDOT, 97 %, Sigma-Aldrich) and iron-III chloride (FeCl<sub>3</sub>, 97 %, Sigma-Aldrich) were used as received. PEDOT was deposited on as-received **500 µm thick** Si (100) 10 cm wafers, fixed facing down at the top part of the reactor on a thermally regulated substrate holder, allowing depositions up to 150 °C. The FeCl<sub>3</sub> powder was placed at the bottom of the reactor on a resistively heated open crucible (2 cm×2 cm×5 mm) and was sublimated at

fixed temperatures. EDOT was placed in a glass jar whose temperature was regulated at 70 °C by immersion in a water bath. Nitrogen, N<sub>2</sub> (99.999 %, Air Liquide) flowing at 10 standard cubic centimeters (sccm) was sent just after the EDOT jar to be used as the carrier gas for the monomer. The operating pressure was fixed at 100 mTorr and was regulated by a gate valve placed at the exit of the reactor, just before a turbo molecular pump (Edwards EXT 250). The leak rate of the reactor was systematically checked before each experiment and was lower than 1 Pa/min. The duration of a deposition experiment was correlated with the exposure time, initiated by simultaneously feeding the reactor with EDOT vapors and heating the FeCl<sub>3</sub> crucible at a constant temperature ( $T_{\text{FeCl}_3}$ ). The consumption of FeCl<sub>3</sub> and EDOT was systematically determined for each experiment by weighting the crucible and the jar, respectively, before and after each experiment, with a KERN ABS 320-4N balance with a precision of 0.1 mg.

### **2.3. Film characterization techniques**

The PEDOT film mass was evaluated by weighting the Si wafers, using a Sartorius R180D balance with a precision of 0.01 mg. For some experiments, immediately after the deposition, substrates were rinsed in methanol (MeOH 99.99 %, Sigma-Aldrich) for 15 min and then dried under N<sub>2</sub>. Although MeOH is not the most efficient solvent for the present case [25], it is the most commonly used one; it is convenient, presents limited interaction with the PEDOT film and in such a way it facilitates the investigation of the process. Experiments corresponding to each set of deposition conditions were reproduced twice.

Film thickness was measured with a stylus profilometer (DektakXT) equipped with a 2 μm stylus tip radius operating under 3 mg load. Measurements were performed on consecutive 1 cm distant points, shown in Fig. 1b along both x and y-axes. Step heights were made on purpose by covering prior deposition a 2 cm large cross-zone of the substrates with a Kapton tape and

then removing it. At each position, the average value of three measurements was considered revealing repeatability within  $\pm 7\%$ . Optical images of film surfaces were obtained with a BX Olympus microscope. The film thickness was analyzed on cross-sections of selected samples by scanning electron microscopy (SEM) (Helios NanoLab 600i), which was also used to investigate the surface morphology from top view micrographs. The topography of the surfaces of the films was investigated by atomic force microscopy (AFM) using an Agilent Technologies AFM/STM 5500 (PicoPlus) instrument.

The film composition was analyzed using transmission Fourier transform infrared spectrometry (FTIR), performed with a PerkinElmer Spotlight 400 with 16 scans at  $4\text{ cm}^{-1}$  resolution. As the analyzed surface is centimetric, the spectra were acquired at the center of each quadrant formed after Kapton removal from the substrate.

Film sheet resistance,  $R_s$  [ $\Omega/\square$ ], was measured with a Signatone S-302-4 four-point probe station on  $2.5 \times 2.5\text{ cm}^2$  coupons cut from the wafer substrates. A constant current of 200 nA was applied with a Keithley 6220 instrument, and the corresponding voltage was read on a Keithley 2182A one. A correction factor of 4.4516 was used in calculating the sheet resistance, as shown in Eq. (1) for cleaved samples [38], where  $V$  is the measured voltage, and  $I$  is the applied current. **Untreated Si wafers systematically showed a sheet resistance of  $35 \pm 5\text{ k}\Omega/\square$ , being significantly high to avoid sheet resistance correction due to parallel conduction of the substrate.** The conductivity ( $\sigma$ ) of the films was evaluated from the  $R_s$  values using Eq. (2), where  $t$  is the local thickness on the film close to each resistivity measurement point. The four-point probe was systematically placed all over the films gathering sheet resistance data. Fifteen sheet resistance measurements were done on each sample. Thickness and sheet resistance profiles were overlaid to estimate the average electrical conductivity of each film.

$$R_s = 4.4516 \frac{V}{I} \quad (1)$$

$$\sigma = \frac{1}{R_s t} \quad (2)$$

### 3. Results and discussion

#### 3.1. In-situ monitoring of film deposition

First, three experiments were performed in the same conditions at  $T_{\text{FeCl}_3}$  and  $T_{\text{sub}}$  equal to 175 °C and 20 °C, respectively, for three different exposure times equal to 3 min, 10 min, and 30 min, with the aim to monitor the stability of the process and the resulting characteristics and properties of the produced PEDOT films.

Table 1 presents the EDOT and  $\text{FeCl}_3$  evaporated masses, and deposition mass, average thickness and average conductivity for the three experiments. The EDOT consumption per unit time for each deposition experiment is constant, equal to 1.5 mg/min, expectedly, meaning a constant flow rate of the monomer. In contrast, the evaporated mass of  $\text{FeCl}_3$  equals 87 mg for the three experiments despite the tenfold difference of the exposure times. We conclude that the oxidant mass does not change with sublimation time and the deposition might occur only during the first 3 min of each experiment. In line with these results, the mass gain of the substrates is *ca.* 0.1 mg, the same for the three experiments. Similarly, the measured thickness and the resulting electrical conductivity are also the same for all experiments, approximately 36 nm and 370 S/cm, respectively. During these experiments, the evolution of the QCM frequency as a function of time was also monitored. The results are presented in Fig. 2a. Fig. 2b will be described in the following sections. For the three experiments, the frequency decreases during the first 3 min, revealing the film formation. Then, for the 10 min and 30 min experiments, it slowly and continuously increases.

**Table 1 EDOT and FeCl<sub>3</sub> evaporated mass, film deposition mass, average thickness and average conductivity for three experiments performed at T<sub>FeCl<sub>3</sub></sub> and T<sub>sub</sub> equal to 175 °C and 20 °C, respectively, for three different exposure times equal to 3 min, 10 min and 30 min.**

Run #	Total exposure time (min)	Evaporated mass of EDOT (g)	Evaporated mass of FeCl <sub>3</sub> (g)	Film mass (mg)	Average thickness (nm)	Average conductivity (S/cm)
1	3	0.0047±0.0002	0.0873±0.0002	0.09±0.02	37±3	372±12
2	10	0.0148±0.0002	0.0872±0.0003	0.09±0.01	35±3	371±8
3	30	0.0439±0.0001	0.0871±0.0001	0.10±0.01	36±5	365±10

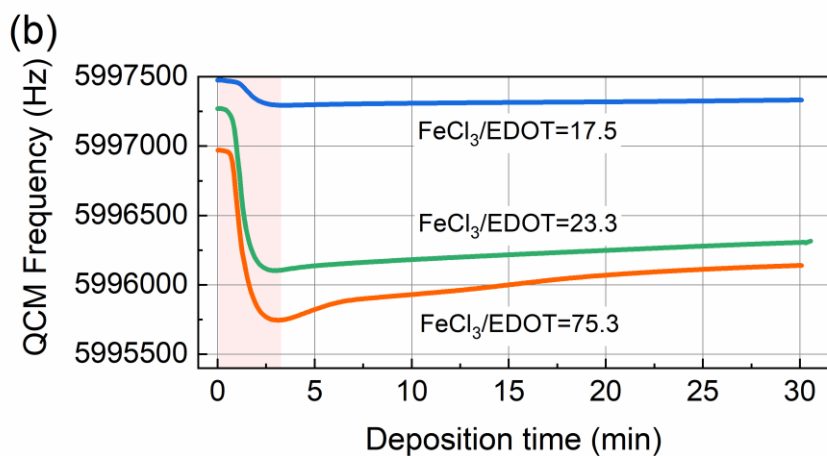
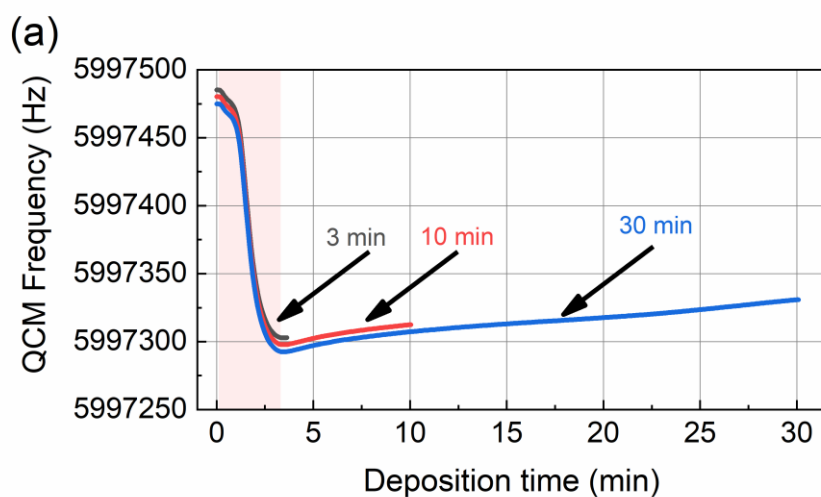


**Fig. 2 (a) Evolution of the QCM frequency with the deposition time for runs #1, #2 and #3, (b) QCM response comparison for three oxidant/monomer ratios in runs #1 to #3 ( $T_{\text{sub}}=20\text{ }^{\circ}\text{C}$ ).**

The mass difference of both the crucible and the substrate for these three experiments concomitantly indicate a discontinuous sublimation of  $\text{FeCl}_3$ , taking place only in the first 3 min of operation. After each experiment, we observed that the  $\text{FeCl}_3$  powder in the crucible was partly sintered and that its color changed from dark grey to red, revealing at least partial superficial transformation [39,40]. **We attribute this behavior to the high sensitivity of the  $\text{FeCl}_3$  powder to moisture contaminations.**

Despite the low leak rate of the reactor, traces of **humidity** contamination can be enough to **superficially hydrolyze**  $\text{FeCl}_3$  at the applied sublimation temperatures, thus blocking its evaporation after a few minutes. As a result, the deposition of the film only occurs during the first 3 min, independently of the exposure time, in agreement with the mass gain of the substrate and the continuous decrease of the frequency of QCM only during the first 3 min of exposure time for the three experiments. Application of various protocol modifications with the aim to reduce the contact with air of the  $\text{FeCl}_3$  powder during its introduction into the reactor, such as suppressing the weighing step, mixing the powder with dried silica powder, introducing it into the reactor under nitrogen flow, did not yield any improvement. The inability of a solid sublimator to deliver at a controlled rate a reproducible and stable flow of vaporized solid precursor is due to several factors such as inefficient heat and mass transfer and, as in the present case, changing specific surface area and alteration of the powdered precursor. Solutions to overcome this commonly met problem have been compiled by Vahlas et al. [41].

The increase of the QCM frequency after 3 min for runs #2 and #3 indicates a continuous mass loss during the last 7 min and 27 min, respectively with, however a smaller slope than that of the frequency decrease during the first 3 min of exposure time. Considering the presence of excess  $\text{FeCl}_3$  on the PEDOT films as it will be presented hereafter, this desorption phenomenon

could be attributed to the conversion of  $\text{FeCl}_3$  to  $\text{FeCl}_2$  [21,35] and to the release of gaseous by-products such as  $\text{HCl}$  or  $\text{Cl}_2$  formed during the PEDOT polymerization in the films [28].

These results indicate that the deposition of PEDOT requires the simultaneous presence of  $\text{FeCl}_3$  and EDOT. This situation is similar to the VPP process, for which the substrate is first coated by an active film of dried  $\text{FeCl}_3$  and vaporized EDOT can react and produce long chains as long as enough oxidant is available on the surface to produce radicals of EDOT [11]. Subsequent exposure to EDOT in the absence of oxidant to create monomer radicals, as is the case for the last 7 and 27 min for runs #2 and #3 does not yield further polymerization. This behavior is compatible with the step growth polymerization (SGP) mechanism [42], as firstly suggested by Gleason et al. [33]. During SGP, the very first functional, i.e., radical monomer, is produced by losing one electron in the presence of the oxidant. During several stepwise reactions, two functional monomers form intermediate components that can react with another monomer molecule or with another intermediate molecule, forming a larger intermediate. These steps continue until the high polymer is obtained. If the oxidant flow rate stops, the monomer can no longer transform into a functional form, and polymerization stops.

Considering an active deposition time of 3 min for runs #1, #2 and #3, the deposition rate is systematically close to 12 nm/min, much higher than that of VPP for the same exposure time [43]. The conductivity reaches 370 S/cm, in line with values reported in the literature for PEDOT oCVD from EDOT and  $\text{FeCl}_3$  [16,21]. It is worth recalling that, in our experiments, the deposition conditions were optimized neither in terms of reactants ratio nor in terms of  $T_{\text{sub}}$  with the aim to increase the conductivity of the films.

### **3.2. Film uniformity and deposition mechanism**

In order to get insight into the PEDOT deposition mechanisms, an experiment was conducted involving eleven  $2 \times 2 \text{ cm}^2$  Si coupons fixed vertically on a scaffold structure into the reactor, as

illustrated in Fig. 3. One-third of each coupon was covered by Kapton tape in order to measure the deposition thickness by profilometry. A Si wafer and clean quartz were also placed on the substrate holder and the microbalance, respectively, as usual in order to compare with the produced film on coupons.  $T_{\text{FeCl}_3}$  and  $T_{\text{sub}}$  were fixed at 175 °C and 20 °C, respectively. The average thickness measured on each coupon is also presented in Fig. 3. The eleven values vary between  $35\pm 7$  and  $39\pm 6$  nm, to be compared with  $36\pm 6$  nm on the Si wafer, indicating uniform deposition all over the reactor. On top of that, the thickness measurement over the quartz surface showed the same thickness of  $36\pm 7$  nm.

Considering that the total pressure is very low, the gaseous diffusivity is high, and the oxidant and EDOT concentrations are identical everywhere into the reactor, provided there is no gas phase reaction. No solid residues were found in the reactor witnessing gas phase reactions. Having similar thickness on eleven coupons means that the deposition rate is identical for all of them on the scaffold even if the residence time to reach each coupon is different. This could indicate that the deposition mechanisms of PEDOT on the surface of the substrates occurs through heterogeneous (surface) reactions and no intermediate species are involved.

Resistivity analysis of samples showed a similar electrical conductivity of  $370\pm 15$  S/cm for all samples. Both values of the electrical conductivity and the thickness are very close to the ones reported in Table 1 for the deposition on Si wafers, indicating the reproducibility of the deposition process.

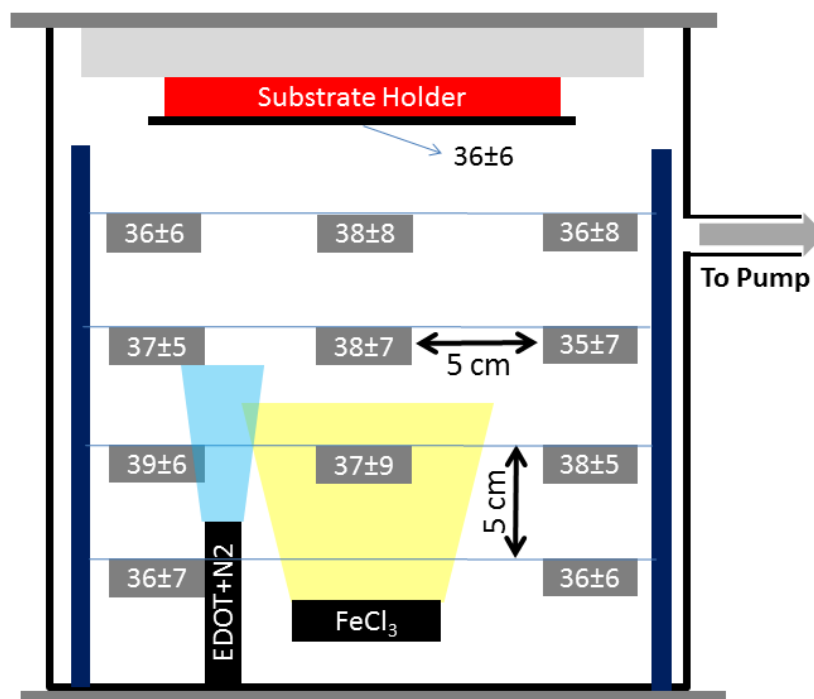


**Fig. 3. Schematic view of the Si coupons placed on a scaffold into the oCVD reactor. The average thickness (in nm) of the deposited PEDOT on each sample is also reported.**

### 3.3. FeCl<sub>3</sub>/EDOT ratio

Since the surface reactions leading to the formation of PEDOT involve both the oxidant and the monomer, it is important to analyze the influence of their ratio on the characteristics and properties of the films. We investigated this parameter by performing three experiments in nominal conditions at  $T_{\text{sub}}=20$  °C for 30 min, with  $T_{\text{FeCl}_3}$  equal 175 °C, 200 °C, and 240 °C. EDOT flow rate was kept at 1.5 mg/min. Fig. 2b presents the QCM frequency response for the three experiments. The frequency systematically decreases during the first 3 min indicating film deposition only during this period. The increase of  $T_{\text{FeCl}_3}$  has no effect on the duration of the sublimation of FeCl<sub>3</sub>. In contrast, increasing the inlet FeCl<sub>3</sub>/EDOT ratio results in a stronger decrease of the QCM frequency, revealing higher deposition rates.

Again, after 3 min, the frequency increases, suggesting desorption of gaseous products from the surface. Desorption is higher when  $T_{\text{FeCl}_3}$  and consequently the  $\text{FeCl}_3/\text{EDOT}$  ratio are higher, suggesting that a higher concentration of  $\text{FeCl}_3$  in the gas phase provides the surface with a larger amount of iron unreacted compounds.

Table 2 presents the evaporated mass of the two reactants. Based on the vaporization behavior of  $\text{FeCl}_3$  observed in Fig. 2b, the reported  $\text{FeCl}_3/\text{EDOT}$  molar ratio in the inlet gas was calculated by dividing by ten the mass of EDOT in order to consider the same vaporization time of 3 minutes for the monomer and the oxidant.

**Table 2 Evaporated mass of EDOT and  $\text{FeCl}_3$  during three deposition experiments performed during 30 min at  $T_{\text{sub}}=20$  °C. Each experiment was performed at different  $T_{\text{FeCl}_3}$ . The last column shows the calculated  $\text{FeCl}_3/\text{EDOT}$  molar ratios in the inlet gas considering that the evaporated mass of EDOT is one-third of that of the reported values.**

Run #	$\text{FeCl}_3$ temperature (°C)	Evaporated EDOT mass in 30 min (g)	Evaporated $\text{FeCl}_3$ mass in 30 min (g)	$\text{FeCl}_3/\text{EDOT}$ molar ratio
3	175	0.0439±0.0001	0.0871±0.0001	17.5
4	200	0.0442±0.0002	0.1168±0.0002	23.3
5	240	0.0441±0.0001	0.3782±0.0002	75.3

The film thickness profiles measured by profilometry locally in the x-direction along the wafer diameter on each substrate are presented in Fig. 4a as a function of the  $\text{FeCl}_3/\text{EDOT}$  ratio. The effect of the rinsing step, often proposed in the literature to remove solid oxidant by-products from the film, is also presented. We observe that the average thickness of the as processed PEDOT films increases with the  $\text{FeCl}_3/\text{EDOT}$  ratio from 36 nm to 261 nm for ratios of 17.5 and 75.3, respectively. After rinsing, the corresponding thicknesses slightly decrease to 33 nm and 248 nm, revealing a minor effect of rinsing. The same evolution is observed in the y-direction on the substrate. The thickness standard deviation on the substrate is 5 % for  $\text{FeCl}_3/\text{EDOT}$  ratio of 17.5, indicating a satisfactory uniformity all over the surface of 10 cm

wafers. It is moderately degraded by increasing the  $\text{FeCl}_3/\text{EDOT}$  ratio to reach 14 % for the ratio of 75.3. The good uniformity observed on the 10 cm substrate for the lowest ratio confirms the results obtained in the previous section about the gas-phase concentration uniformity and surfacic deposition mechanisms.

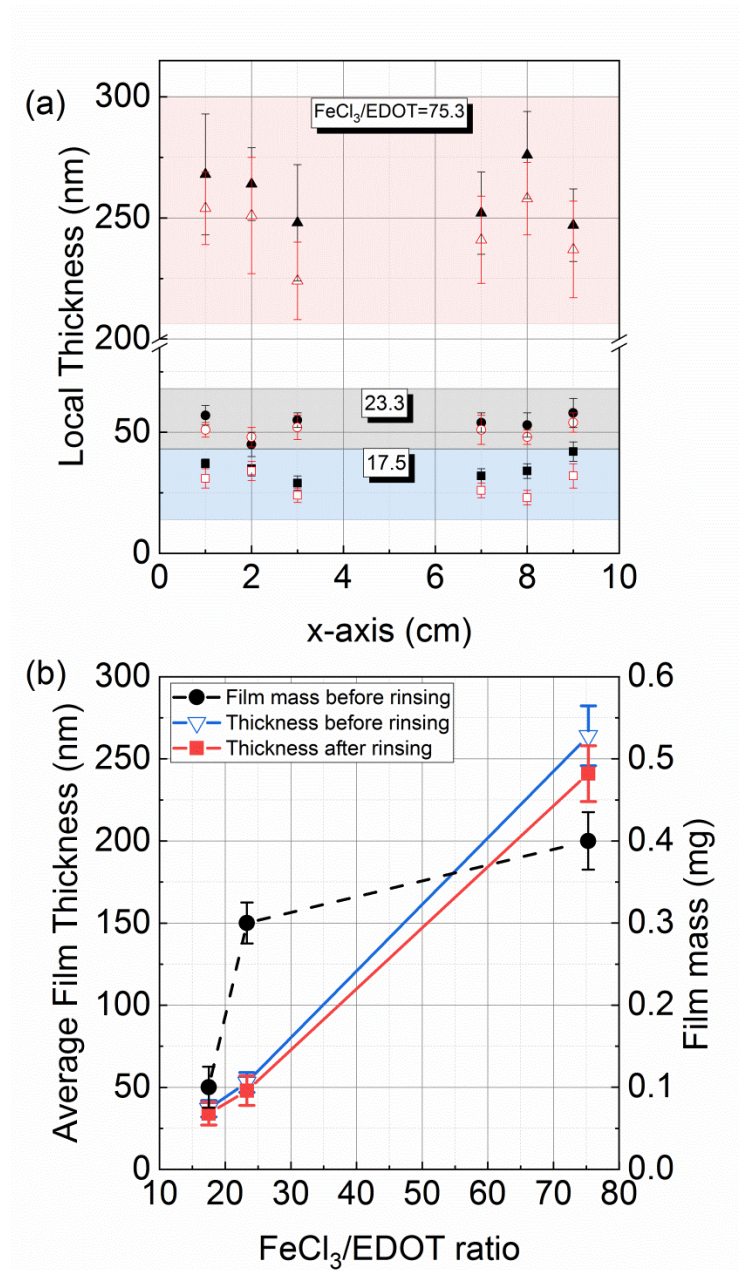


**Fig. 4 (a) Thickness profiles measured on the substrates in the x-direction for the three  $\text{FeCl}_3/\text{EDOT}$  ratios before (full symbols) and after (empty symbols) rinsing. (b) Influence of the  $\text{FeCl}_3/\text{EDOT}$  ratio on deposition mass before rinsing and thickness evolution before (blue) and after (red).**

Fig. 4b details the influence of the  $\text{FeCl}_3/\text{EDOT}$  ratio on the average film thickness and mass on each substrate before and after rinsing. The film thickness increases from 36 nm to 265 nm, with the oxidant/monomer ratio. Similar behavior was observed in the literature for PEDOT films deposited **at low substrate temperature** [16]. The deposited mass also increases, but with decreasing slope at higher  $\text{FeCl}_3/\text{EDOT}$  values. As a result, the apparent density decreases from approximately  $850 \text{ kg/m}^3$  for the  $\text{FeCl}_3/\text{EDOT}$  ratios of 17.5 and 23.3 to  $250 \text{ kg/m}^3$  for the ratio of 75.3. The former value is similar to reported ones for VPP PEDOT [11] and PEDOT:PSS [44]. These values are the first apparent densities determined for oCVD PEDOT. We attribute the decrease of the density with increasing the oxidant to monomer ratio to the evolution of the composition and/or to the increase of the porosity of the films. Indeed, due to its negligible vapor pressure at  $T_{\text{sub}}=20 \text{ }^\circ\text{C}$ , gaseous  $\text{FeCl}_3$  can be easily condensed on the surfaces since its partial pressure in the adopted sublimation conditions largely exceeds its saturated vapor pressure near the substrate.

The surface morphology of the films before rinsing is shown in Fig. 5 from SEM images at two different magnifications.

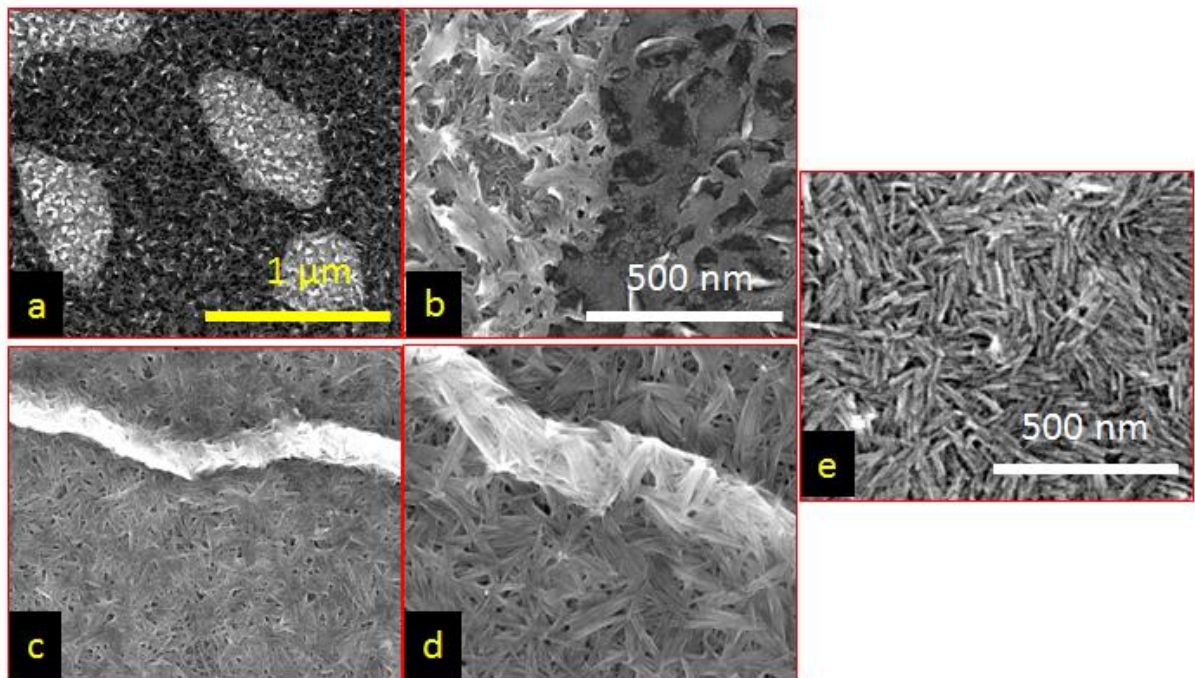


**Fig. 5 SEM surface micrographs of as processed PEDOT films deposited at  $T_{\text{sub}}=20\text{ }^{\circ}\text{C}$  at  $\text{FeCl}_3/\text{EDOT}$  ratios 17.5 (a, b) and 75.3 (c, d). A surface micrograph of a  $\text{FeCl}_3$  film condensed on the Si wafer in absence of EDOT is shown for comparison (e). The scale for (a and c) is  $1\mu\text{m}$  while it is  $500\text{ nm}$  for (b, d and e).**

It can be seen that the surface morphology of PEDOT films is highly dependent on the  $\text{FeCl}_3/\text{EDOT}$  ratio. For the lowest ratio tested, at low magnification (Fig. 5a), two distinct regions can be observed: a continuous dark zone on which brighter micronic nodules are present. Fig. 5b shows that these bright zones exhibit a needle-like structure, whereas dark zones are more continuous with some pores. The morphology of films processed at the intermediate  $\text{FeCl}_3/\text{EDOT}$  ratio is similar, with smaller and more numerous bright islands (not presented). At the highest ratio, (Fig. 5c and Fig. 5d), the morphology is different, more uniform with a localized presence of bright lines which seems to be cracks or creases (fold). For comparison, Fig. 5e presents the surface of a  $\text{FeCl}_3$  film condensed on the Si surface upon sublimation in the same conditions as in run #5 ( $T_{\text{FeCl}_3} = 240\text{ }^{\circ}\text{C}$ ) without EDOT flux. This morphology, made of tangles of needles, is close to that of Fig. 5c and Fig. 5d, and to the bright

zones in Fig. 5a and Fig. 5b. This similarity indicates the systematic presence of unreacted  $\text{FeCl}_3$  or derivatives on the surface of PEDOT films. **Zuber et al. found that in the PEDOT VPP process from Fe(III) tosylate, the oxidant reacting with water could form crystallites which are non active for polymerization [45].** In the presence of EDOT, the needles seem more significant, as if PEDOT coated the needles or grew from or around them. Fig. 6 presents optical, AFM, and SEM surface micrographs, before and after rinsing, of a film obtained for the lowest  $\text{FeCl}_3/\text{EDOT}$  ratio (17.5). The bright nodules observed by SEM are also shown on the optical micrographs (Fig. 6a) and AFM topography images (Fig. 6c). On optical micrographs, they exhibit various colors in contrast to the continuous background phase (dark zone on SEM), with shimmer effects on the edges of the domains, characteristic of thickness variations of thin films. The thickness difference between the continuous dark phase and micronic nodules is confirmed by the AFM topography image, where the height of the nodules above the continuous phase is approximately 80 nm. It is interesting to note that these nodules are removed during the rinsing step (Fig. 6b and Fig. 6d), leading to a flatter surface with more uniform morphology, as shown in SEM images in Fig. 6e and Fig. 6f. These nodules were not detected during thickness determination by profilometry experiments operating in contact mode, probably due to the non-cohesive or viscous behavior of the matter in these domains. Indeed, during profilometry measurements, the stylus passed through these iron-containing islands and the reported values for the thickness only concern the continuous film of PEDOT. In contrast, AFM operating in tapping mode does not deform the surface topography of such samples and allows measuring the thickness over such Fe-rich islands without any deposition modification.

As the saturated vapor pressure of  $\text{FeCl}_3$  at 20 °C is very low [46], the excess  $\text{FeCl}_3$ ; i.e., not participating in the formation of PEDOT, could condensate on the film during its deposition and partly decompose into sub-chlorides which, in turn, could be hydrolyzed to iron hydroxides upon exposure to air. These results indicate that the investigated  $\text{FeCl}_3/\text{EDOT}$  ratios are

systematically larger than the optimum one resulting in films with the highest electrical conductivity and lowest impurities.

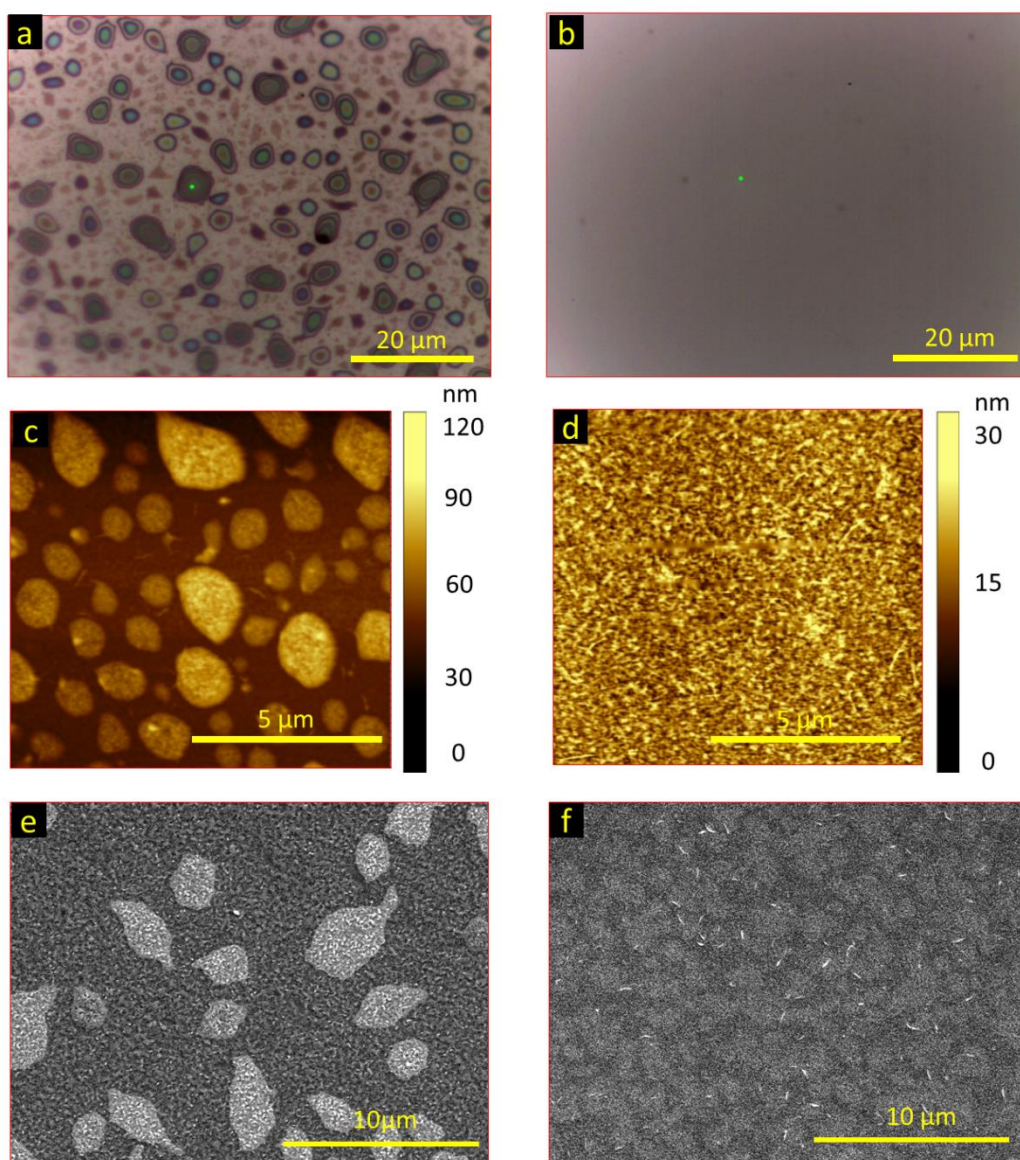


**Fig. 6 Optical microscopy images (a, b), AFM surface micrographs (c, d) and SEM surface micrographs (e, f) of PEDOT films processed at  $T_{\text{sub}}=20\text{ }^{\circ}\text{C}$  and  $\text{FeCl}_3/\text{EDOT}$  ratio of 17.5 (run #3). The left and right columns correspond to as processed and to rinsed samples, respectively.**

Fig. 7a shows the FTIR spectra of the PEDOT films after rinsing, normalized to the C-O-C peak at  $1082\text{ cm}^{-1}$ . Vibrations are observed at 1520, 1319, 1184, 1138, 1082, 1043, 972, 915, 832 and  $682\text{ cm}^{-1}$ . Those at 1520 and  $1319\text{ cm}^{-1}$  are assigned to the asymmetric stretching mode of C=C and intra-ring stretching mode of C-C in the thiophene ring, respectively. The ones at

1184, 1138, 1082, and 1043  $\text{cm}^{-1}$  are attributed to the C–O–C bending vibration in ethylenedioxy group, while those at 972, 915, 832, and 674  $\text{cm}^{-1}$  are characteristic peaks of stretching vibrations of the C–S bond in thiophene ring, which confirms the successful formation of PEDOT [47-49]. The C–H vibration at 3100  $\text{cm}^{-1}$  reported in the monomer spectrum disappears in the spectra of the polymer, confirming the successful polymerization of the EDOT molecules. Vibrations at 3380 and 1620  $\text{cm}^{-1}$  are commonly associated with OH bonds in the film [50]. The observed peaks correspond to previously published data for PEDOT [13] and confirm the formation of PEDOT for all investigated conditions.

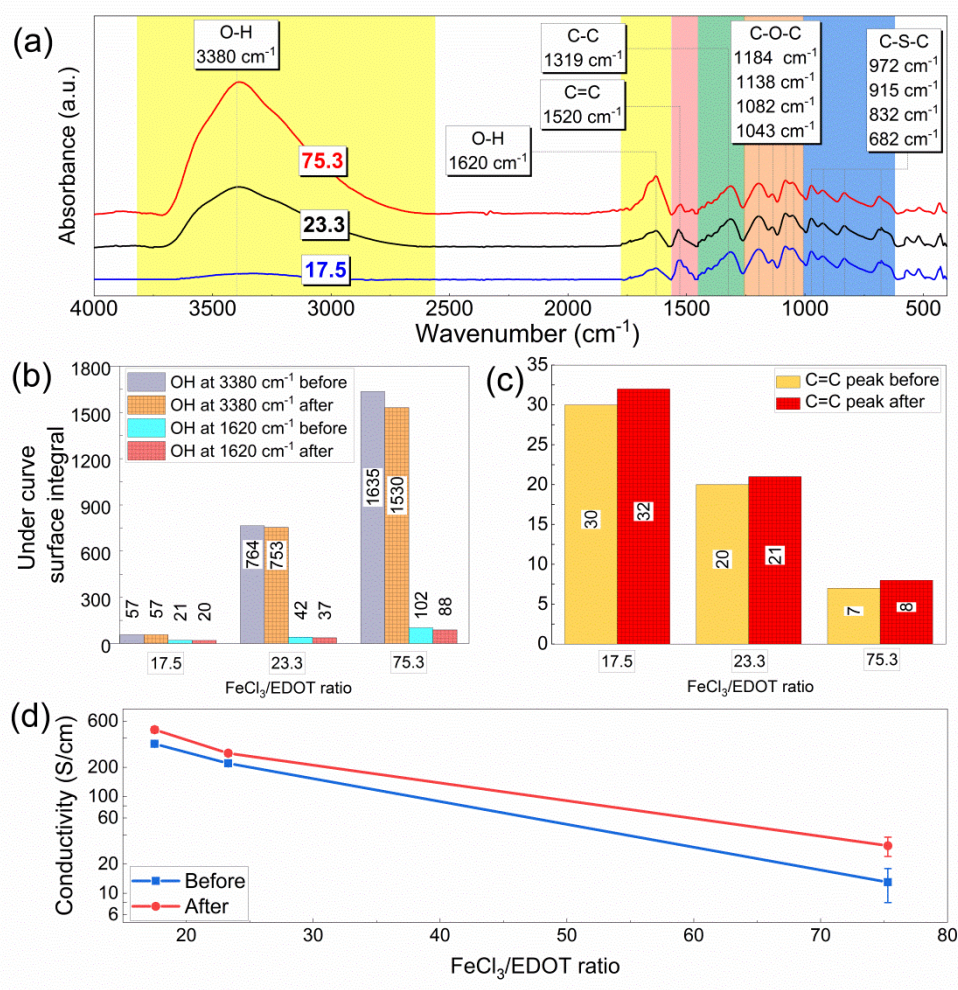


**Fig. 7** For the three investigated FeCl<sub>3</sub>/EDOT ratios, (a) FTIR spectra of PEDOT films after rinsing. (b) Under curve surfaces of OH peaks at 1620 and 3380  $\text{cm}^{-1}$  before and after rinsing. (c) Under curve

**surfaces of the C=C peak at 1520 cm<sup>-1</sup> before and after rinsing. (d) Evolution of the electrical conductivity before and after rinsing.**

Most of the PEDOT peaks do not demonstrate any change in relative intensity with the FeCl<sub>3</sub>/EDOT ratio, except for the ones at 3380, 1620 cm<sup>-1</sup> corresponding to OH bonds and at 1520 cm<sup>-1</sup> corresponding to the asymmetric stretching mode of C=C. We found no significant difference in the FTIR spectra after rinsing. Fig. 7b and Fig. 7c highlight the areas under the peaks at 3380 and 1620 cm<sup>-1</sup> (left) and 1520 cm<sup>-1</sup> (right) for non-rinsed samples. The under peak area of the C=C stretching mode at 1520 cm<sup>-1</sup> decreases from 30 to 7 with increasing the FeCl<sub>3</sub>/EDOT ratio from 17.5 to 75.3. For the 3380 and 1620 cm<sup>-1</sup> peaks, these areas increase with increasing the FeCl<sub>3</sub>/EDOT ratio before and after rinsing while the area decreases for the stretch peak at 1520 cm<sup>-1</sup>. Together, they suggest less iron oxide products for the sample with the ratio of 17.5 and the presence of more C=C bonds in the back chain, respectively.

The OH bond peaks may be attributed to the hygroscopic nature of iron (sub-)chlorides, resulting in the formation of, e.g., Fe(OH)<sub>2</sub> or Fe<sub>2</sub>O<sub>3</sub>, which have already been observed in such films [51]. Indeed, unreacted FeCl<sub>3</sub> may be present on the surface of the films for the highest FeCl<sub>3</sub>/EDOT ratios tested, which leads to the formation of larger amounts of iron oxides. This confirms the interpretation of the AFM results for run #3, where iron-containing islands were formed over the PEDOT film. Interestingly, the corresponding two peaks at 3380 and 1620 cm<sup>-1</sup> present slightly lower intensities after rinsing in MeOH, suggesting that iron-containing species are not wiped out entirely and can still absorb humidity. This result confirms that MeOH is not optimal in removing these undesired products, in agreement with the dedicated work by Howden et al. [25]. It also shows that it is necessary to optimize the deposition conditions in order to minimize the condensation of excess FeCl<sub>3</sub> and, consequently, to avoid the post deposition rinsing step.

Fig. 7d presents the evolution of the electrical conductivity of the films as a function of the FeCl<sub>3</sub>/EDOT ratio, before and after rinsing. A small improvement of conductivity is observed after rinsing, in agreement with previously reported results [9,22,25]. It is correlated to a small increase in the under peak area of the C=C bond after rinsing. This improvement of the conductivity could also be due to the partial removal of iron byproducts. Increasing the FeCl<sub>3</sub>/EDOT ratio from 17.5 to 75.3 results in a decrease of the conductivity from 500 to 12 S/cm after rinsing. This demonstrates that the FeCl<sub>3</sub>/EDOT ratio is a key parameter to optimize the film conductivity.

Fig. 7c shows that the intensity of the C=C peak at 1520 cm<sup>-1</sup> decreases by increasing the FeCl<sub>3</sub>/EDOT ratio. The charge transfer in conductive polymers can be a function of several parameters, including polymer chain length, crystallinity, polymer conjugation length and impurities [4]. It has been reported that the intensity of the C=C peak at 1520 cm<sup>-1</sup> on the FTIR spectra increases with increasing the conjugation length of PEDOT [13] and that such an increase enhances the electrical conductivity of conductive polymers [52]. Our conductivity measurements are in agreement with the conjugation length decrease. Zhao et al. reported a similar trend using direct polymerization of PEDOT, namely an increase of the conjugation length by reducing the FeCl<sub>3</sub>/EDOT ratio [53]. For the same T<sub>sub</sub> and total pressure, sending 3 sccm of EDOT and sublimating the oxidant at 320 °C, Im and Gleason reported a conductivity of 0.05 S/cm after rinsing in methanol [13]. This lower value, in comparison with the present results, is indeed attributed to the larger excess of FeCl<sub>3</sub> in their case.

It should be pointed out that the conductivity variations observed in our study are limited within one decade, to be compared with reported results on PEDOT films spanning within five decades. This might be due to the small range of the investigated FeCl<sub>3</sub>/EDOT ratio. Taking into account the previously presented uncertainties of the thickness measurements, this relative stability highlights the robustness of the oCVD process for the production of conductive PEDOT films.

### 3.4. Substrate temperature

The parametric investigation of the oCVD of PEDOT films is mainly focused on the variation of  $T_{\text{sub}}$  [9,16,22,23,29,32,33]. For example, Im et al. [14] reported that increasing  $T_{\text{sub}}$  from 15 °C to 100 °C allows increasing the electrical conductivity of the film from 1 S/cm to 350 S/cm. They associated this improvement to the longer conjugation length and the higher doping level of the films processed at high  $T_{\text{sub}}$  [13,14]. Drewelow et al. recently observed the same trend reaching conductivities at  $T_{\text{sub}}=100$  °C as high as 2440 S/cm when applying a multi-step post deposition rinsing and drying protocol [16].

Three  $T_{\text{sub}}$  of 20 °C, 70 °C and 100 °C were studied for  $T_{\text{FeCl}_3}$  equal to 175 °C. Fig. 8a presents the obtained average film thickness and mass. Both film thickness and mass increase with  $T_{\text{sub}}$ . This trend is somehow contrary to the overall observation by Drewelow et al., who operated at 8 mTorr [16]. The authors attributed the observed behavior to the higher vapor pressure of  $\text{FeCl}_3$  near the substrate at higher  $T_{\text{sub}}$ , which became higher than their  $\text{FeCl}_3$  partial pressure, with subsequent limited surface adsorption. In our case, the total pressure is higher (100 mTorr), leading to partial pressures of  $\text{FeCl}_3$  near the substrate high enough to exceed the saturated vapor pressure of  $\text{FeCl}_3$  even at 100°C, thus suppressing any limitation of surface adsorption. The deposition rate is seemingly reaction-rate limited between 20 and 70 °C, as  $T_{\text{sub}}$  controls it. Again, a slight decrease in thickness is observed after rinsing. The film's apparent density increases from 850 kg/m<sup>3</sup> at 20 °C to 910 kg/m<sup>3</sup> and 1000 kg/m<sup>3</sup> by heating the substrate respectively at 70 °C and 100 °C. This could indicate that the porosity of the films decreases when  $T_{\text{sub}}$  is increased. Fig. 8b shows the evolution of the electrical conductivity of the PEDOT films as a function of  $T_{\text{sub}}$ . In agreement with reported results [54], the conductivity of the as-processed films increases from 360 S/cm at 20 °C to 1100 S/cm at 100 °C. A minor

improvement of the conductivity is observed for all  $T_{\text{sub}}$  after methanol rinsing. The highest electrical conductivity obtained is 1350 S/cm at 100 °C after rinsing.

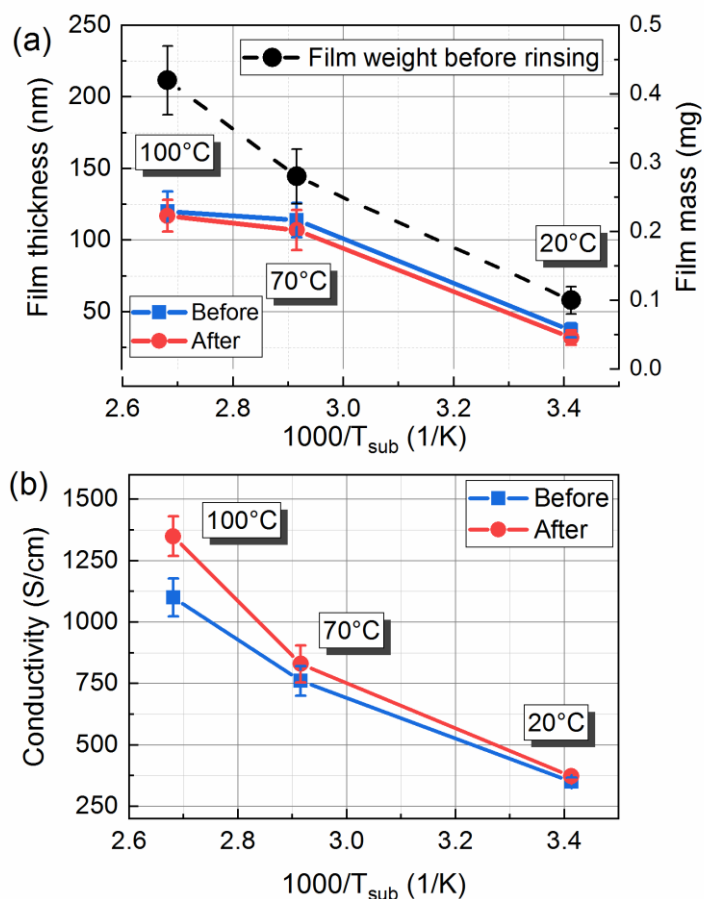


**Fig. 8 Evolution of the deposition rate (a) and the electrical conductivity (b) as a function of  $T_{\text{sub}}$ .**

Fig. 9a shows the FTIR spectra of the films deposited at the three  $T_{\text{sub}}$ . The spectra are comparable, with minor differences concerning the intensity of the peak of the C=C conjugation peak at  $1520\text{ cm}^{-1}$ , which increases with  $T_{\text{sub}}$ , similarly to the literature [13,14]. Also, the films deposited at high  $T_{\text{sub}}$  present weaker peaks relative to OH groups containing species, namely those at  $3400\text{ cm}^{-1}$  and  $1600\text{ cm}^{-1}$ . The histograms of Fig. 9b quantify these trends. Heating the substrate from 20 °C to 100 °C increases the under curve area for the C=C peak at  $1520\text{ cm}^{-1}$

from 30 to 55 while it reduces the under curve area of OH peaks from 57 to almost zero. It can be concluded that the rearrangement of the conjugated bonds is in agreement with the increase of electrical conductivity for films processed at higher  $T_{\text{sub}}$ . Moreover, heating the substrate reduces the condensation of the excess  $\text{FeCl}_3$  during deposition, which also contributes to the improvement of the conductivity.

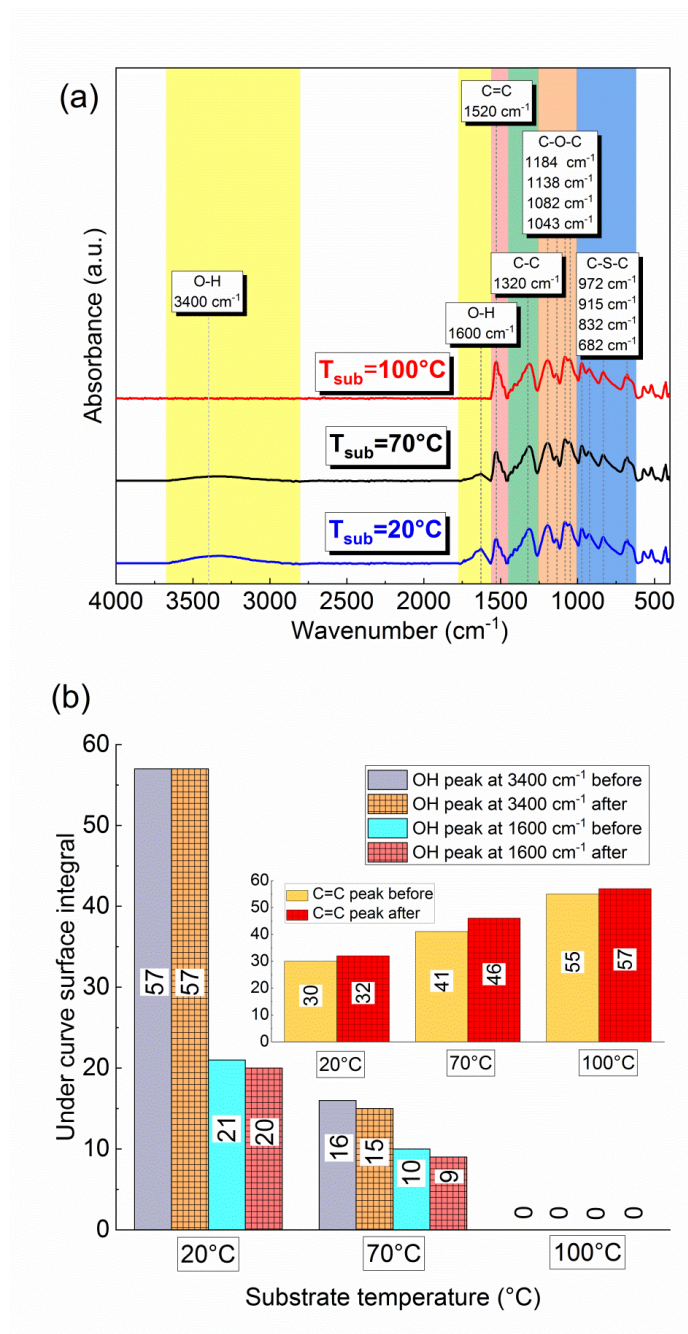


**Fig. 9 (a) FTIR spectra of PEDOT films as a function of  $T_{\text{sub}}$  after rinsing, (b) Comparison of under curve surfaces of OH and C=C peaks before and after rinsing.**

Fig. 10 presents surface SEM micrographs of the films deposited at the three investigated  $T_{\text{sub}}$ . The film morphology clearly depends on the **substrate temperature**. A two-phase morphology prevails at  $T_{\text{sub}}=20\text{ }^{\circ}\text{C}$ , depicted by isolated bright areas surrounded by a dark grey continuum. The entire morphology of the films is characterized by an acicular microstructure, characteristic of condensed, unreacted  $\text{FeCl}_3$ . Increasing  $T_{\text{sub}}$  to  $70\text{ }^{\circ}\text{C}$  results in a sharp decrease of the bright areas and, at the same time, in morphological coarsening of the continuous grey one. The bright zones disappear at  $100\text{ }^{\circ}\text{C}$  (Fig 10c). At this  $T_{\text{sub}}$ , the acicular microstructure disappears, in agreement with the FTIR results, where less OH bonds were visible for higher substrate temperatures. The film seems more homogeneous and continuous at  $100\text{ }^{\circ}\text{C}$ . However, it is difficult to conclude from these micrographs about a possible decrease in the film porosity with increasing  $T_{\text{sub}}$ .

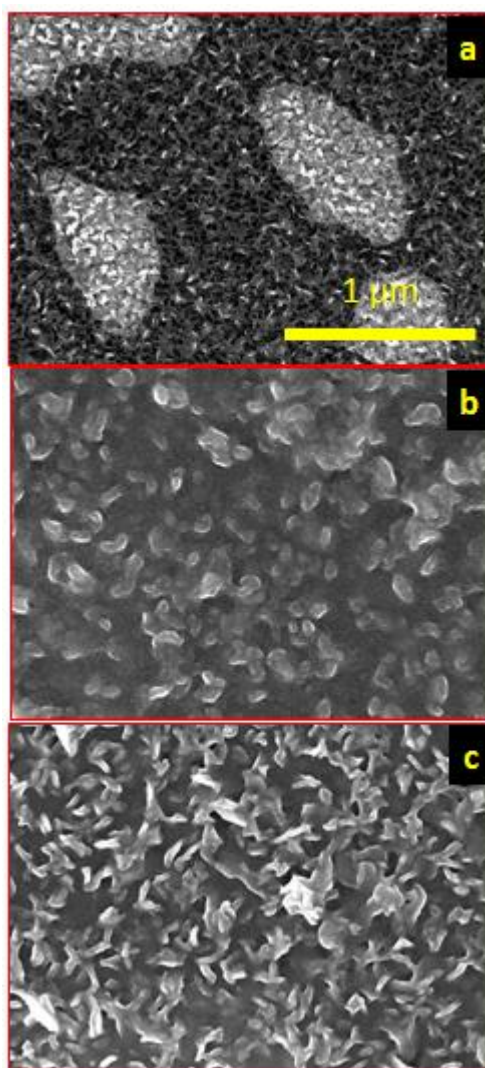


**Fig. 10** Surface SEM micrographs of PEDOT films deposited at (a)  $T_{\text{sub}}=20$  °C, (b)  $T_{\text{sub}}=70$  °C and (c)  $T_{\text{sub}}=100$  °C. The scale is 1  $\mu\text{m}$ .

#### **4. Conclusions**

In this work, we revisit the oCVD process for the deposition of PEDOT films from EDOT and  $\text{FeCl}_3$  in standard process conditions, including 100 mTorr and 20 to 100 °C operating pressure and substrate temperature, respectively. The combination of an *in situ* Quartz Crystal Microbalance and the determination of the EDOT and the  $\text{FeCl}_3$  consumption for each experiment revealed a discontinuous  $\text{FeCl}_3$  evaporation rate in a standard sublimation hardware architecture often reported in the literature. Simultaneous deposition on 10 cm silicon wafers

and coupons positioned on a large-scale scaffold demonstrates that film thickness and electrical conductivity are uniform, independently of the location in the reactor. It also illustrated the absence of gas-phase reactions and intermediate species in the polymerization of PEDOT. The enhanced gas diffusivity prevailing in the adopted process conditions favors a purely surface PEDOT deposition mechanism occurring through step growth polymerization. Such a mechanism, based on heterogeneous reactions, allows in turn deposition of uniform PEDOT films over large and/or complex substrates.

Detailed correlations between the deposition conditions and the film thickness, weight, chemical composition, morphology, and electrical conductivity were established for various  $\text{FeCl}_3$ /EDOT inlet ratios and substrate temperatures.

This work brings an out of the box vision of the oCVD of PEDOT films from sublimed solid oxidants. It reveals the hard points of the process, and in such, it paves the way towards highly conductive oCVD PEDOT films processed from convenient solid oxidants. New studies are in progress to develop a setup ensuring a constant flow rate of oxidant and to optimize the oxidant/monomer ratio to reduce contaminations in PEDOT and suppressing the rinsing step.

## **Conflicts of interest**

There are no conflicts to declare.

## **Acknowledgments**

We are indebted to C. Tendero and O. Marsan (CIRIMAT), C. Josse and T. Hungria (UMS Castaing), and M.L. de Solan Bethmale (LGC SAP) for their contribution concerning sample characterizations. We would like to thank J. Compain (LGC), E. Prevot (LGC), D. Samelor, and D. Sadowski (CIRIMAT) for their help in preparing the experimental setup.

## References

- [1] F. Brunetti, A. Operamolla, S. Castro-Hermosa, G. Lucarelli, V. Manca, G.M. Farinola, T.M. Brown, Printed solar cells and energy storage devices on paper substrates, *Adv. Funct. Mater.*, 29 (2019) 1806798. <https://doi.org/10.1002/adfm.201806798>.
- [2] Z. Wang, L. Gao, X. Wei, M. Zhao, Y. Miao, X. Zhang, H. Zhang, H. Wang, Y. Hao, B. Xu, Energy level engineering of PEDOT: PSS by antimonene quantum sheet doping for highly efficient OLEDs, *J. Mater. Chem. C*, 8 (2020) 1796-1802. <https://doi.org/10.1039/C9TC06049A>.
- [3] G. Fabregat, L. Hodásová, L.J. del Valle, F. Estrany, C. Alemán, Sustainable Solid-State Supercapacitors Made of 3D-Poly (3, 4-ethylenedioxythiophene) and  $\kappa$ -Carrageenan Biohydrogel, *Adv. Eng. Mater.*, 20 (2018) 1800018. <https://doi.org/10.1002/adem.201800018>.
- [4] A. Elschner, S. Kirchmeyer, W. Lovenich, U. Merker, K. Reuter, PEDOT: principles and applications of an intrinsically conductive polymer, CRC Press, USA, 2010.
- [5] B. Cho, K.S. Park, J. Baek, H.S. Oh, Y.-E. Koo Lee, M.M. Sung, Single-crystal poly (3, 4-ethylenedioxythiophene) nanowires with ultrahigh conductivity, *Nano Lett.*, 14 (2014) 3321-3327. <https://doi.org/10.1021/nl500748y>.
- [6] C.E. Carraher Jr, Carraher's polymer chemistry, CRC Press, Florida, USA, 2017.
- [7] E. Genies, G. Bidan, A. Diaz, Spectroelectrochemical study of polypyrrole films, *J. Electroanal. Chem. Interfacial Electrochem.*, 149 (1983) 101-113. [https://doi.org/10.1016/S0022-0728\(83\)80561-0](https://doi.org/10.1016/S0022-0728(83)80561-0).
- [8] S. Kirchmeyer, K. Reuter, Scientific importance, properties and growing applications of poly (3, 4-ethylenedioxythiophene), *J. Mater. Chem.*, 15 (2005) 2077-2088. <https://doi.org/10.1039/B417803N>
- [9] J.P. Lock, S.G. Im, K.K. Gleason, Oxidative chemical vapor deposition of electrically conducting poly (3, 4-ethylenedioxythiophene) films, *Macromolecules*, 39 (2006) 5326-5329. <https://doi.org/10.1021/ma060113o>.
- [10] J. Kim, E. Kim, Y. Won, H. Lee, K. Suh, The preparation and characteristics of conductive poly (3, 4-ethylenedioxythiophene) thin film by vapor-phase polymerization, *Synth. Met.*, 139 (2003) 485-489. [https://doi.org/10.1016/S0379-6779\(03\)00202-9](https://doi.org/10.1016/S0379-6779(03)00202-9).

- [11] M.A. Ali, K.-H. Wu, J. McEwan, J. Lee, Translated structural morphology of conductive polymer nanofilms synthesized by vapor phase polymerization, *Synth. Met.*, 244 (2018) 113-119. <https://doi.org/10.1016/j.synthmet.2018.07.007>.
- [12] M.C. Barr, C. Carbonera, R. Po, V. Bulović, K.K. Gleason, Cathode buffer layers based on vacuum and solution deposited poly (3, 4-ethylenedioxythiophene) for efficient inverted organic solar cells, *Appl. Phys. Lett.*, 100 (2012) 97. <https://doi.org/10.1063/1.4709481>.
- [13] S.G. Im, K.K. Gleason, Systematic control of the electrical conductivity of poly (3, 4-ethylenedioxythiophene) via oxidative chemical vapor deposition, *Macromolecules*, 40 (2007) 6552-6556. <https://doi.org/10.1021/ma0628477>.
- [14] S.G. Im, K.K. Gleason, E.A. Olivetti, Doping level and work function control in oxidative chemical vapor deposited poly (3, 4-ethylenedioxythiophene), *Appl. Phys. Lett.*, 90 (2007) 152112. <https://doi.org/10.1063/1.2721376>.
- [15] S.P. Arnold, J.K. Harris, B. Neelamraju, M. Rudolph, E.L. Ratcliff, Microstructure-dependent electrochemical properties of chemical-vapor deposited poly (3, 4-ethylenedioxythiophene)(PEDOT) films, *Synth. Met.*, 253 (2019) 26-33. <https://doi.org/10.1016/j.synthmet.2019.04.022>.
- [16] G. Drewelow, H.W. Song, Z.-T. Jiang, S. Lee, Factors Controlling Conductivity of PEDOT Deposited Using Oxidative Chemical Vapor Deposition, *Appl. Surf. Sci.*, (2019) 144105. <https://doi.org/10.1016/j.apsusc.2019.144105>.
- [17] D. Bhattacharyya, K.K. Gleason, Low band gap conformal polyselenophene thin films by oxidative chemical vapor deposition, *J. Mater. Chem.*, 22 (2012) 405-410. <https://doi.org/10.1039/C1JM13755G>.
- [18] D.C. Borrelli, S. Lee, K.K. Gleason, Optoelectronic properties of polythiophene thin films and organic TFTs fabricated by oxidative chemical vapor deposition, *J. Mater. Chem. C*, 2 (2014) 7223-7231. <https://doi.org/10.1039/C4TC00881B>.
- [19] H. Chelawat, S. Vaddiraju, K. Gleason, Conformal, conducting poly (3, 4-ethylenedioxythiophene) thin films deposited using bromine as the oxidant in a completely dry oxidative chemical vapor deposition process, *Chem. Mater.*, 22 (2010) 2864-2868. <https://doi.org/10.1021/cm100092c>.
- [20] N. Chen, X. Wang, K.K. Gleason, Conformal single-layer encapsulation of PEDOT at low substrate temperature, *Appl. Surf. Sci.*, 323 (2014) 2-6. <https://doi.org/10.1016/j.apsusc.2014.06.123>.

- [21] N. Cheng, L. Zhang, J.J. Kim, T.L. Andrew, Vapor phase organic chemistry to deposit conjugated polymer films on arbitrary substrates, *J. Mater. Chem. C*, 5 (2017) 5787-5796. <https://doi.org/10.1039/C7TC00293A>
- [22] S.G. Im, D. Kusters, W. Choi, S.H. Baxamusa, M. Van de Sanden, K.K. Gleason, Conformal coverage of poly (3, 4-ethylenedioxythiophene) films with tunable nanoporosity via oxidative chemical vapor deposition, *ACS Nano*, 2 (2008) 1959-1967. <https://doi.org/10.1021/nm800380e>.
- [23] P. Kovacik, G. del Hierro, W. Livernois, K.K. Gleason, Scale-up of oCVD: large-area conductive polymer thin films for next-generation electronics, *Mater. Horiz.*, 2 (2015) 221-227. <https://doi.org/10.1039/C4MH00222A>
- [24] J.P. Lock, J.L. Lutkenhaus, N.S. Zacharia, S.G. Im, P.T. Hammond, K.K. Gleason, Electrochemical investigation of PEDOT films deposited via CVD for electrochromic applications, *Synth. Met.*, 157 (2007) 894-898. <https://doi.org/10.1016/j.synthmet.2007.08.022>.
- [25] R.M. Howden, E.D. McVay, K.K. Gleason, oCVD poly (3, 4-ethylenedioxythiophene) conductivity and lifetime enhancement via acid rinse dopant exchange, *J. Mater. Chem. A*, 1 (2013) 1334-1340. <https://doi.org/10.1039/C2TA00321J>.
- [26] B. Pistillo, K. Mengueli, N. Desbenoit, D. Arl, R. Leturcq, O. Ishchenko, M. Kunat, P. Baumann, D. Lenoble, One step deposition of PEDOT films by plasma radicals assisted polymerization via chemical vapour deposition, *J. Mater. Chem. C*, 4 (2016) 5617-5625. <https://doi.org/10.1039/C6TC00181E>
- [27] D. Farka, A.O. Jones, R. Menon, N.S. Sariciftci, P. Stadler, Metallic conductivity beyond the Mott minimum in PEDOT: Sulphate at low temperatures, *Synth. Met.*, 240 (2018) 59-66. <https://doi.org/10.1016/j.synthmet.2018.03.015>.
- [28] S.E. Atanasov, M.D. Losego, B. Gong, E. Sachet, J.-P. Maria, P.S. Williams, G.N. Parsons, Highly conductive and conformal poly (3, 4-ethylenedioxythiophene)(PEDOT) thin films via oxidative molecular layer deposition, *Chem. Mater.*, 26 (2014) 3471-3478. <https://doi.org/10.1021/cm500825b>.
- [29] S. Kaviani, M. Mohammadi Ghaleni, E. Tavakoli, S. Nejati, Electroactive and Conformal Coatings of oCVD Polymers for Oxygen Electroreduction, *ACS Appl. Polym. Mater.*, (2019) <https://doi.org/10.1021/acsapm.8b00240>.
- [30] M. Heydari Gharahcheshmeh, K. Gleason, *Using volatile liquid oxidant in PEDOT synthesis by oxidative Chemical Vapor Deposition (oCVD)*, in *APS Meeting Abstracts*. 2019.

- [31] M.H. Gharahcheshmeh, M.M. Tavakoli, E.F. Gleason, M.T. Robinson, J. Kong, K.K. Gleason, Tuning, optimization, and perovskite solar cell device integration of ultrathin poly (3, 4-ethylene dioxythiophene) films via a single-step all-dry process, *Sci. Adv.*, 5 (2019) eaay0414. <https://doi.org/10.1126/sciadv.aay0414>.
- [32] M. Heydari Gharahcheshmeh, K.K. Gleason, Device Fabrication Based on Oxidative Chemical Vapor Deposition (oCVD) Synthesis of Conducting Polymers and Related Conjugated Organic Materials, *Adv. Mater. Interfaces*, 6 (2019) 1801564. <https://doi.org/10.1002/admi.201801564>.
- [33] K.K. Gleason, *CVD Polymers: Fabrication of Organic Surfaces and Devices*, John Wiley & Sons, 2015.
- [34] W.E. Tenhaeff, K.K. Gleason, Initiated and oxidative chemical vapor deposition of polymeric thin films: iCVD and oCVD, *Adv. Funct. Mater.*, 18 (2008) 979-992. <https://doi.org/10.1002/adfm.200701479>.
- [35] D. Bilger, S.Z. Homayounfar, T.L. Andrew, A critical review of reactive vapor deposition for conjugated polymer synthesis, *J. Mater. Chem. C*, 7 (2019) 7159-7174. <https://doi.org/10.1039/C9TC01388A>.
- [36] S.G. Im, *Oxidative and initiated chemical vapor deposition for application to organic electronics*. 2009, Massachusetts Institute of Technology.
- [37] G.G. Genchi, G. Ciofani, Smart Tools for Caring: Nanotechnology Meets Medical Challenges, 7 (2019) 11.
- [38] F. Smits, Measurement of sheet resistivities with the four-point probe, *Bell Syst. Tech. J.*, 37 (1958) 711-718. <https://doi.org/10.1002/j.1538-7305.1958.tb03883.x>.
- [39] K.A. Strohfeldt, *Essentials of inorganic chemistry: For students of pharmacy, pharmaceutical sciences and medicinal chemistry*, John Wiley & Sons, 2015.
- [40] R.M. Cornell, U. Schwertmann, *The iron oxides: structure, properties, reactions, occurrences and uses*, John Wiley & Sons, 2003.
- [41] C. Vahlas, B. Caussat, W. L Gladfelter, F. Senocq, E. J Gladfelter, Liquid and solid precursor delivery systems in gas phase processes, *Recent Pat. Mater. Sci.*, 8 (2015) 91-108. <http://dx.doi.org/10.2174/1874464808666150324230711>.
- [42] D.M. Teegarden, *Polymer chemistry: introduction to an indispensable science*, NSTA Press, 2004.

- [43] P.A. Levermore, L. Chen, X. Wang, R. Das, D.D. Bradley, Fabrication of highly conductive poly (3, 4-ethylenedioxythiophene) films by vapor phase polymerization and their application in efficient organic light-emitting diodes, *Adv. Mater.*, 19 (2007) 2379-2385. <https://doi.org/10.1002/adma.200700614>.
- [44] F. Zabihi, Y. Xie, S. Gao, M. Eslamian, Morphology, conductivity, and wetting characteristics of PEDOT: PSS thin films deposited by spin and spray coating, *Appl. Surf. Sci.*, 338 (2015) 163-177. <https://doi.org/10.1016/j.apsusc.2015.02.128>.
- [45] K. Zuber, M. Fabretto, C. Hall, P. Murphy, Improved PEDOT conductivity via suppression of crystallite formation in Fe (III) tosylate during vapor phase polymerization, 29 (2008) 1503-1508.
- [46] S. Blairs, Sublimation study of anhydrous ferric chloride, *J. Chem. Thermodyn.*, 38 (2006) 1484-1488. <https://doi.org/10.1016/j.jct.2005.12.012>.
- [47] Y.-H. Cheng, C.-W. Kung, L.-Y. Chou, R. Vittal, K.-C. Ho, Poly (3, 4-ethylenedioxythiophene)(PEDOT) hollow microflowers and their application for nitrite sensing, *Sens. Actuators, B*, 192 (2014) 762-768. <https://doi.org/10.1016/j.snb.2013.10.126>.
- [48] C. Deetuan, C. Samthong, S. Thongyai, P. Prasertdam, A. Somwangthanaroj, Synthesis of well dispersed graphene in conjugated poly (3, 4-ethylenedioxythiophene): polystyrene sulfonate via click chemistry, *Compos. Sci. Technol.*, 93 (2014) 1-8. <https://doi.org/10.1016/j.compscitech.2013.12.024>.
- [49] Y. Xiao, J. Wu, G. Yue, J. Lin, M. Huang, Z. Lan, L. Fan, Electrodeposition of high performance PEDOT/Ti counter electrodes on Ti meshes for large-area flexible dye-sensitized solar cells, *Electrochim. Acta*, 85 (2012) 432-437. <https://doi.org/10.1016/j.electacta.2012.08.077>.
- [50] H. Günzler, H.-U. Gremlich, IR spectroscopy. An introduction, Wiley-VCH, Germany, 2002.
- [51] S. Lee, D.C. Paine, K.K. Gleason, Heavily Doped poly (3, 4-ethylenedioxythiophene) Thin Films with High Carrier Mobility Deposited Using Oxidative CVD: Conductivity Stability and Carrier Transport, *Adv. Funct. Mater.*, 24 (2014) 7187-7196. <https://doi.org/10.1002/adfm.201401282>.
- [52] R. Baughman, L. Shacklette, Conjugation length dependent transport in conducting polymers from a resistor network model, *J. Chem. Phys.*, 90 (1989) 7492-7504. <https://doi.org/10.1063/1.456183>.

- [53] Q. Zhao, R. Jamal, L. Zhang, M. Wang, T. Abdiryim, The structure and properties of PEDOT synthesized by template-free solution method, *Nanoscale Res. Lett.*, 9 (2014) 557. <https://doi.org/10.1186/1556-276X-9-557>.
- [54] P.M. Smith, L. Su, W. Gong, N. Nakamura, B. Reeja-Jayan, S. Shen, Thermal conductivity of poly (3, 4-ethylenedioxythiophene) films engineered by oxidative chemical vapor deposition (oCVD), *RSC Adv.*, 8 (2018) 19348-19352. <https://doi.org/10.1039/C8RA03302A>.